Korean J. Chem. Eng.
DOI: 10.1007/s11814-020-0667-2

pISSN: 0256-1115
eISSN: 1975-7220

Kinetic study of activation and deactivation of adsorbed cellulase during enzymatic conversion of alkaline peroxide oxidation-pretreated corn cob to sugar

Augustine Omoniyi Ayeni*,†, Oluranti Agboola*, Michael Olawale Daramola, Bianca Grabner***, Babalola Aisosa Oni*, Damilola Elizabeth Babatunde*, and Joseph Evwodere***

*Covenant University, College of Engineering, Department of Chemical Engineering, Canaan land, Ota, Nigeria
**Department of Chemical Engineering, Faculty of Engineering, Built Environment and Information Technology, University of Pretoria, Hatfield, Pretoria 0028, South Africa
***Institute of Process and Particle Engineering, Graz University of Technology, Graz, Austria
(*Received 1 June 2020 • Revised 10 August 2020 • Accepted 21 August 2020*)

Abstract−Corn cob lignocellulosic biomass is one of the useful precursors for the alternative production of fuels and chemicals. Understanding the kinetics of enzymatic conversion of corn cob through kinetic models could provide in-depth knowledge and increase the predictive ability for process design and optimization. In this study, models based on the semi-mechanistic rate equations, first-order decay exponential function of time for adsorbed enzymes, structural and diffusion coefficient for adsorption were used to estimate kinetic parameters for the enzymatic conversion of alkaline peroxide oxidation (APO) pretreated corn cob to sugar. Fitting a first-order inactivation model of adsorbed cellulases to account for experimental hydrolysis data, the apparent hydrolysis rate constant (k_2=29.51 min^{-1}), the inactivation rate constant (k_3=0.269 min^{-1}), and reactivation rate constant (k_4=0.0048 min^{-1}) were estimated. Regressed values of apparent maximum rate, $V_{max,\,app}$, for adsorbed enzymes reduced appreciably with time to more than 98% at 96 h. The diffusion limit model showed that the diffusion resistance increased with increasing enzyme concentrations.

Keywords: Lignocellulose, Kinetic Models, Enzymatic Hydrolysis, Adsorption, Inactivation

INTRODUCTION

Recently, there has been global attention to alternative sources for fuels and chemicals [1,2]. Lignocellulosic biomasses are economically viable alternative materials for the production of platform chemicals, biofuels, and other value-added bioproducts derived from them [3-6]. Some of the derived biobased products from lignocelluloses include sorbitol, succinic acid, sugars, levulinic acid ethanol, butanol, and lactic acid [7]. Corncob is the central solid part of corn (*Zea mays*) that accounts for 16%-19% of the whole corn [8]. All over the world, corn cob as a non-edible lignocellulosic material is useful in the production of bio-commodities, renewable, and clean energy [9]. However, many technical and economic difficulties hinder the development of biobased products from biomass [10]. Enzyme hydrolysis on treated lignocelluloses is an efficient, economical, and mild way of producing sugars amenable to further downstream processing [11-13]. The optimization of the enzymatic conversion process of lignocelluloses requires adequate knowledge of the kinetics of the reaction. The nature and the structure of the cellulolytic enzymes play crucial roles in the development of enzymatic kinetic models [14]. Kinetic modelling of enzymatic conversion of lignocelluloses is a challenging area of bioreactor engineering science because of the difficulties in the complexity of the substrate, action of the enzyme, enzyme-substrate interaction, and multiple effects of the enzyme complex [15]. Deactivation of cellulase enzymes during enzymatic hydrolysis process slows the hydrolysis rate [16]. The slow kinetics and the reduction in the rate of conversion to valuable products stand as bottlenecks [10,11,17,18] for a viable production process. Factors that may be responsible for cellulase deactivation include ineffective adsorption of cellulase, temperature, product inhibition, ion strength, non-productive binding caused by the presence of lignin [19], and shear force [20]. Change in substrate properties, such as crystallinity [18], accessibility [21-24], can cause rate reduction. Also, low product concentration, high cost of enzymes, misinterpretation, and misunderstanding of the cellulose kinetics on substrates are significant challenges to enzymatic hydrolysis [11]. Several kinetic models have been developed from experimental studies with discrepancies in the reported results. Hence, the need to have an in-depth understanding of the kinetic study via both experimental and modelling approaches.

This kinetic study centred on three approaches to assess how enzyme kinetic models conform to the experimental data for the APO pretreated corn cob biomass. The first approach was based on the classical nonlinear model of Michaelis-Menten (c-MM) along with the linearized forms (Lineweaver-Burke (LB), Langmuir, and Eadie-Hofstee (EH)), and the modified MM model (m-MM) to estimate kinetic parameters: the maximum initial hydrolysis rate of product formation (V_{max}), and the Michaelis-Mentens constant (k_m) which describes the formation and dissociation of the enzyme-substrate complex, of the enzymatic process [12,15,25]. In the second approach, experimental data were fitted to kinetic models to account

†To whom correspondence should be addressed.
E-mail: augustine.ayeni@covenantuniversity.edu.ng, aoayeni@gmail.com

for the apparent hydrolysis rate ($V_{max,app}$), the deactivation rate constant (k_3), and the reactivation rate constant (k_4) values of the adsorbed cellulase on substrates [10,20]. Finally, the Chrastil model [26,27] was applied to evaluate the diffusion characteristics of the enzymatic process by estimating the kinetic parameters k (rate constant, which is proportional to the diffusion coefficient for adsorption) and n (the structural diffusion resistant constant). These kinetic parameters provided adequate understanding, prediction, and enabled us to evaluate the effects of the addition, removal, or modification of the process components as they may affect the design of a bioreactor.

MATERIALS AND METHODS

1. Materials Sourcing and Preparation

Corn cob (*Zea mays*) residues were harvested from farmland around Iju town, near Ota (6°40′N 3°08′E), South West, Nigeria. The samples were prepared after collection, as described elsewhere [9]. Using a band saw, the cobs were reduced and further shredded in a rotor mill having a 4 mm sieve. Samples were screened through different laboratory sieve sizes. Screened samples were dried in a convection oven at 105 °C for 3 h and kept in plastic bottles. Samples were stored in a locker in the laboratory until they were ready to be used. The corn cob particle sizes used for this study ranged between 0.3 mm to 2.36 mm. Sodium hydroxide, hydrogen peroxide (35%w/v), D(+)-glucose, cellulase enzyme (*Trichoderma reesei*, with the specific enzyme activity of 700 units g^{-1} were purchased from Sigma-Aldrich (Chemie GmbH).

2. Biomass Pretreatment

The raw biomass was subjected to initial pretreatment to disrupt the lignocellulosic complex held together by lignin and be exposed to a better enzymatic attack. Samples were subjected to thermal heating in an oven. Pretreatment operating variables were as follows: 12.5 g corn cob biomass loading to the liquid volume of 250 mL distilled water, 1%(v/v) H_2O_2, and 0.05 gNaOH g^{-1} biomass addition to taking the mixture to pH of 11.5 [28]. The raw biomass was initially soaked for 24 h under ambient temperature (23 °C) in the sodium hydroxide-hydrogen peroxide mixture before the heating process. Reactions occurred at a specified pretreatment temperature of 80 °C and a time of 2 h. At the end of the pretreatment, slurries were separated into solid and liquid fractions through vacuum filtration. Solid fractions were washed to a pH of 7. A portion of the wet solid was used to estimate the conversion of the treated material by cellulase enzymes and to measure the reducing sugar production as the equivalent of glucose concentration. The composition (cellulose, hemicellulose, lignin, extractives, and ash content) of the raw biomass was estimated by the method as reported elsewhere [29]. Dissolved oxygen content in the mixture was measured before and after pretreatment with YSI Professional Plus (Pro Plus) multiparameter testing instrument.

3. Enzyme Hydrolysis

Commercial preparation of *Trichoderma reesei*, ATCC 2692 (with subunits of 68 kiloDalton) cellulases, was added at a loading of 25 FPU·g biomass^{-1}. Kinetic parameters were determined at varying substrate concentration of 5, 20, 30, 40, and 50 g·L^{-1} and initial enzyme concentration of 7, 14, 21, 28, and 35 g·L^{-1}. In a shaking incubator (at 300 rpm), pretreated mixtures were hydrolyzed at 50 °C, varying periods of 6, 12, 24, 48, 72, and 96 h. In all the enzyme hydrolysis reactions, constant values of pH (4.8), 0.1 M sodium citrate buffer, and total hydrolysis volume of 10 mL were maintained. 0.5 mL aliquot was withdrawn for each sampling period for product formation and characterized through the dinitrosalycilic assay [30].

The enzymatic conversion yield (%), or %digestibility, was estimated by using Eq. (1), expressed in terms of total polysaccharide in the treated substrate [31,32].

$$\text{Conversion yield (\%)} = \frac{\text{Reducing sugar obatained}\left(\frac{g}{g}\right)\times 0.9}{\text{Treated substrate (cellulose + hemicellulose)}\left(\frac{g}{g}\right)}\times 100 \quad (1)$$

Also, in understanding the progression of product (reducing sugar) formation, an empirical second-order exponential decay, Eq. (2), was used to fit formation of product as a function of reaction time [10,33], using the experimental data.

$$P = P_o + A_1 \text{ x } \exp\left(\frac{-t}{t_1}\right) + A_2 \text{ x } \exp\left(\frac{-t}{t_2}\right) \quad (2)$$

where P is product released (g·L^{-1}), t is reaction time (h), P_o (g·L^{-1}), A_1 (g·L^{-1}), A_2 (g·L^{-1}), t_1 (h), and t_2 (h) are empirical parameters.

4. Enzyme Mechanism and Kinetics

4-1. c-MM and m-MM Semi-mechanistic Models

For enzymatic reactions, an enzyme-substrate complex in equilibrium with the free enzyme and substrate can be described by the Michaelis-Menten mechanism, Eq. (3). The enzyme, E, reacts with a substrate, S, to form an E-S complex, which is a reversible process. The complex E-S converts to form product P. Also, the activation or inactivation of adsorbed enzymes can be described to follow the mechanism as given in Eq. (3).

$$\begin{array}{ccccc} E + S & \underset{k_{-1}}{\overset{k_1}{\rightleftharpoons}} & E\text{-}S_{active} & \xrightarrow{k_2} & E + P \\ & & \underset{k_4}{\overset{k_3}{\rightleftharpoons}} & & \\ & & E\text{-}S_{inactive} & & \end{array} \quad (3)$$

k_1 is the forward reaction rate constant, k_{-1} is the backward reaction rate constant (decomposition of E-S to E and S), k_3=inactivation rate constant, and k_4=reactivation rate constant

From Eq. (3),

$$k_2 = k_{cat} \text{ and } k_m = \frac{k_{-1} + k_2}{k_1}$$

k_2=kcat is the unimolecular rate constant (the turnover number) for the enzyme conversion process of the E-S complex into product P; releasing the enzyme, E. k_m, and k_2 indicates how suitably an enzyme will react with a particular substrate. The quantity, k_2/k_m, is referred to as the catalytic efficiency (which is the rate of efficiency of how the substrate unbinds from the enzyme to form a product). It is a useful measure of the overall efficiency of the catalyst and determines whether the rate is limited by product forma-

tion or the substrate in the reaction environment [34,35]. A low value of k_m or high value of k_2/k_m [35], and the value of the coefficient of determination (R^2) close to unity indicate that the rate efficiency of the process is high.

The pseudo-homogeneous nonlinear Michaelis-Menten (c-MM) model, given as Eq. (4), is the most common semi-mechanistic approach [12,15]:

$$V_o = \frac{d(P)}{dt} = \frac{V_{max}[S]}{k_m + [S]} \tag{4}$$

where V_o=initial hydrolysis rate, [P]=product concentration, [S]=substrate concentration, V_{max}=maximum initial hydrolysis rate of product formation. k_m=MM constant and is the mixture of the rate constants (Eq. (3)) that describes the formation and dissociation of the enzyme-substrate complex [36]. It is also the half-maximum initial velocity rate (i.e., $k_m = {}^1/_2 V_{max}$). k_m gives a sense of the affinity of the enzyme for the substrate. The c-MM model assesses the substrate (despite being a solid) as a soluble reactant by measuring the concentration with the reaction taking place on a hydrated solid [12,15]. When the enzymatic reaction is not diffusion limited, the c-MM model is not applicable for the analysis of heterogeneous structures [26,27]. In resolving the limitation of the c-MM model, a modified semi-mechanistic rate equation of Michaelis-Menten, m-MM, Eq. (5), was proposed [25] by considering the substrate to be in solid form and the enzyme as soluble, which either adsorbs on the substrate or desorbs from it [12,15].

$$V_o = \frac{d[P]}{dt} = \frac{V_{emax}[Eo]}{k_e + [Eo]} \tag{5}$$

where Eo=initial enzyme concentration. V_{emax}=maximum reaction rate. k_e=half-maximum initial velocity rate. V_{max} is as defined in Eqs. (4) and (5). It is related to the first-order rate constant, k_2, and the total enzyme concentration, $[E]_{total}$, (Eq. (6)):

$$V_{max} = k_2[E]_{total} \tag{6}$$

4-2. Deactivation and Reactivation Reaction Rate Mechanism

The decline in enzyme activity can be represented by the inactivation or deactivation of the adsorbed enzyme on the substrates. Deactivation of adsorbed enzymes may be assumed to be due to the formation of a complex with the product.

From Eq. (3),

$$V = \frac{dP}{dt} = k_2[ES] \tag{7}$$

Defining the real hydrolysis rate [10] by considering the cellulase activity loss:

$$V_r = \frac{dP}{dt} = k_2 ES_{active} \tag{8}$$

Relating (7) and (8),

$$\frac{V_r}{V} = \frac{k_2 ES_{active}}{k_2[ES]} \tag{9}$$

$$V_r = V_{max} \times \frac{[S]}{k_m + [S]} \times \frac{[ES]_{active}}{[ES]} \tag{10}$$

Defining,

$$\frac{[ES]_{active}}{[ES]} = Z_0 + B_0 + \exp\left(\ln 2 \times \frac{-t}{t_{1/2}}\right) \tag{11}$$

$$V_r = V_{max} \times \frac{[S]}{k_m + [S]} \times Z_0 + B_0 + \exp\left(\ln 2 \times \frac{-t}{t_{1/2}}\right) \tag{12}$$

where B_0=inactivation extent, Z_0=residual activity of enzyme, $t_{1/2}$=half-life. They are related to the inactivation rate constant, k_3, and reactivation rate constant, k_4.

$$B_0 = \frac{k_3}{k_3 + k_4} \tag{13}$$

$$Z_0 = \frac{k_4}{k_3 + k_4} \tag{14}$$

$$t_{1/2} = \frac{\ln 2}{k_3 + k_4} \tag{15}$$

Defining the apparent V_{max}:

$$V_{max,\,app} = V_{max} \times \left[Z_0 + B_0 \times \exp\left(\ln 2 \times \frac{-t}{t_{1/2}}\right)\right] \tag{16}$$

From Eq. (16), the apparent V_{max} decreases with a first-order exponential decay function of time due to inactivation of the adsorbed enzyme [10],

$$\text{where, } V_r = \frac{dP}{dt} = V_{max,\,app} \times \frac{[S]}{k_m + [S]} \tag{17}$$

Eq. (17) is the reduction of the real hydrolysis rate due to the inactivation of adsorbed enzyme.

4-3. Diffusion Coefficient for Enzyme Adsorption

The rate constant (k), which is proportional to the diffusion coefficient for adsorption, and the structural diffusion resistant constant (n) were obtained from the Chrastil model, Eq. (18). This equation allows the enzymatic reactions to be considered diffusion-limited [12,27], which makes the enzymatic periods depend on the heterogeneous rate-limiting structures of the substrate-enzyme system [12,27]. Chrastil [27] proposed the diffusion-limited kinetic model as:

$$P = P_\sigma [1 - EXP(-kE_o t)]^n \tag{18}$$

where P and P_σ are the products that diffused at every considered time t and equilibrium, respectively. k is the rate constant proportional to the diffusion coefficient defined by Fick's law [37]. E_o is the initial enzyme concentration and n structural diffusion resistance constant dependent on the sterical structure of the system as given by Chrastil and Wilson [26] and Chrastil [27].

The kinetic parameter values for the nonlinear models were optimized through regression by finding the minimum objective function, the sum of the square errors.

5. Physico-chemical Assessment of Raw and Treated Biomass

The physical appearance of the raw and treated samples was monitored by subjecting the dried samples to stereomicroscope imaging. Untreated and treated samples were captured on a black background using a Nikon SMZ745T stereomicroscope [38] attached with NIS-Element D Z-Series 7 software. A Nikon Digital Sight

System operated the Nikon DS-Fi2 CCD camera fixed to the stereomicroscope. To examine the surface morphological changes brought about by APO pretreatment and enzyme hydrolysis on the raw sample, corn cob biomass samples were fixed on aluminum stubs with conductive carbon tape. Biomass particles were sputter-coated with gold-palladium and carbon at a 5 nm scale to minimize charging. The samples were examined with the FEI Quanta 200 scanning electron microscope (SEM). The operating vacuum in the SEM was between 3.9×10^{-4} to 2.2×10^{-3} Pascals with a voltage of 30 kV.

Fourier transform infrared spectroscopy (FTIR) was used to determine the presence of functional groups and obtain related information about the structural changes. Parameters like HBI (hydrogen bonding index which is related to O-H stretching vibrations from alcohols and carboxylic acids present in the structure), LOI (lateral order index which measures the crystallinity and corresponds to a CH_2 bending vibration), and TCI (total crystallinity index which corresponds to the C-H stretching) were used to determine the effectiveness of the pretreatment and enzyme-treated processes [35]. Dried samples were mixed with KBr and pressed under vacuum to form pellets. Spectra analysis was performed at the wavelength range of 4,000-350 cm^{-1} and 64 scans with baseline corrections [39].

All experiments were replicated twice; reported data show mean values of the replicated experiments.

Table 1. Chemical composition (%w/w) of raw and alkaline peroxide oxidation pretreated corn cob biomass

Component	Raw	Pretreated
Cellulose	33.69	54.92
Hemicellulose	28.24	12.92
Lignin	30.53	20.21
Ash	4.49	2.41
Extractives	3.05	8.54

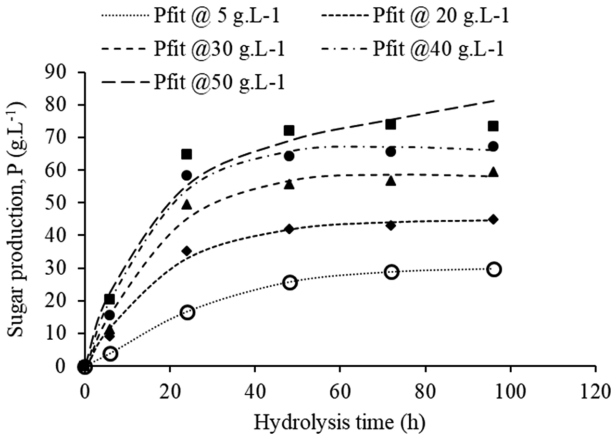

Fig. 1. Product formation as a function of reaction time. Markers represent the experimental data.

RESULTS AND DISCUSSION

1. Effect of APO Pretreatment on Product Yields

The pretreatment process often leads to loss of carbohydrates as the average length of the cellulose chain is decreased. The APO process improves the delignification process. Various conjugate oxygen species are involved during delignification [40], brought about by the series of reduction to water by oxygen. The presence of oxygen serves to reduce the cellulosic chain scission, thereby exposing the monomeric and dimeric cellulose chains to more enzymatic attack. The chemical compositions of raw and treated biomass is presented in Table 1. Pretreatment of raw biomass showed that about 34% of initial lignin content was removed. Cellulosic content enhancement was about 39% from an initial cellulose raw value of 33.69%w/w (Table 1).

The maximum reaction rate is attained once the substrate molecules completely saturate the available enzymes' active sites. Many factors may hinder the maximum production of sugars during enzymatic hydrolysis [13]. Therefore, a single optimum is not possible to define [29]. The optimum may shift depending on factors such as mass transfer and product inhibition [10], dry solid content, pH, temperature, enzyme activity, and desired residence time [29]. The product formation using Eq. (2) [10,33], evaluated based on enzymatic conversion of 5-50 $g{\cdot}L^{-1}$ substrate loadings with varying hydrolysis periods (6-96 h), showed that reducing sugars production increased with increasing substrate loading up to a maximum (Fig. 1). The parameters which represent the regression coefficients in Eq. (2) are provided in Table 2. Product formation attained the maximum at 48 h hydrolysis time (Fig. 1), for all substrate loadings. An optimized substrate loading is necessary for maximum efficiency of the biocatalyst for maximum product yields. Increasing substrate concentration beyond a point can cause product inhibition or inefficient mixing.

The second-order exponential decay equation fitted well to the experimental data within the 5-40 $g{\cdot}L^{-1}$ substrate loading (Fig. 1) and R^2 of 0.9880 to 1 (Table 2), which agrees with other fitting curves

Table 2. The second-order exponential decay fitting parameters for the product formation with hydrolysis time

Substrate concentration (g/L)	P_o ($g{\cdot}L^{-1}$)	A_1 ($g{\cdot}L^{-1}$)	t_1 (h)	A_2 ($g{\cdot}L^{-1}$)	t_2 (h)	R^2
5	30.21	28.71	11.28	−58.92	19.27	1.000
20	44.81	1.43	14.20	−47.76	17.48	0.9912
30	53.24	15.45	89.30	−71.18	18.84	0.9842
40	51.23	23.5	218.41	−77.08	16.72	0.9880
50	31.97	30.94	206.56	−63.01	14.03	0.9683

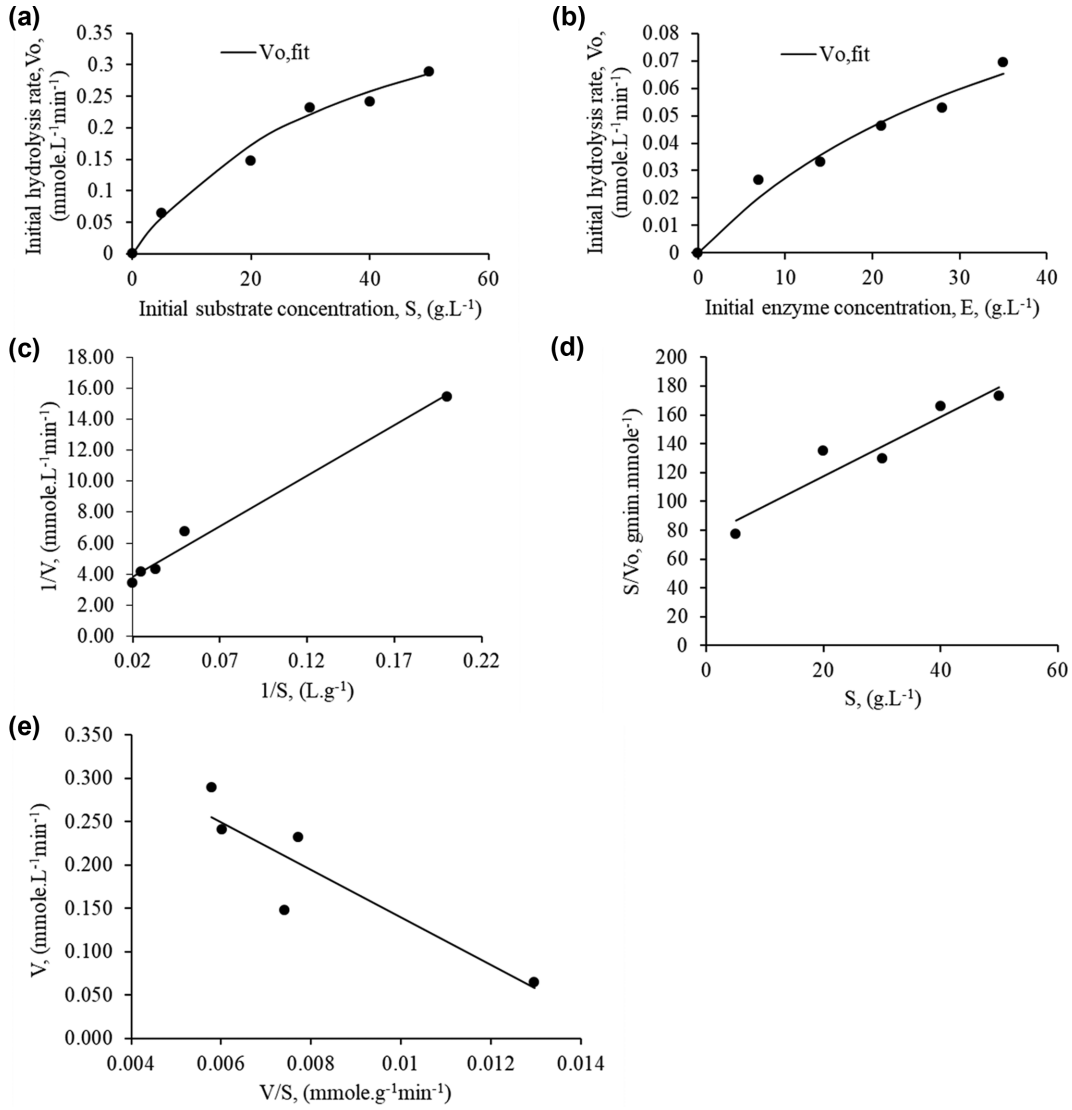

Fig. 2. Substrate concentration on the initial hydrolysis rate for the APO pretreated corn cob. Pretreatment conditions: 2 h, Temp.=80 °C, 1% (v·v^{-1}) H_2O_2, 0.05 gNaOH·g biomass^{-1} loading. Enzymatic hydrolysis conditions: Temp.=50 °C. The line curves are the model fits for (a) c-MM, (b) m-MM, (c) LB, (d) Langmuir, and (e) EH. Markers represent the experimental data.

for product formation previously reported in the literature [10,33,41].

Using Eq. (1), the conversion yield (%) was highest at 48 h for 20 g·L^{-1} (51.8%), 30 g·L^{-1} (68.5%), 40 g·L^{-1} (79.3%), and 50 g·L^{-1} (88.9%). Optimum %conversion yield for 5 g·L^{-1} was 35.7% after 72 h. The conversion yield (%) remained constant after the optimum hydrolysis period (48 h) for all the substrate concentrations. The obtained results after the enzymatic conversion process indicated that the maximum conversion of the pretreated corn cob to sugars occurred at 48 h. Therefore, considering the economy of the enzymatic conversion, hydrolysis beyond 48 h would not be favorable.

2. Estimation of Kinetic Parameters

2-1. c-MM, m-MM, and the Linearized Models

The feasibility of the c-MM and m-MM nonlinear models and the linearized forms of LB, Langmuir, and EH was evaluated using the experimental data for the cellulase enzyme conversion process (considering the initial velocity rate of product formation for substrate loadings (5-50 g·L^{-1}) and hydrolysis periods, 6-96 h). The fitted curves for the variation of the initial velocity rate with initial substrate concentration for the c-MM and m-MM models and the linearized models of LB, Langmuir, and EH are given in Fig. 2. The values for the k_m and V_{max} obtained from the different mod-

Table 3. Semi-mechanistic kinetic model values from regression analysis of experimental results

Parameters	V_{max} (mmole·L^{-1}min^{-1})	k_m (g·L^{-1})	R^2
c-MM	0.51	38.84	0.9850
m-MM	0.15	43.81	0.9722
L-B	0.39	25.49	0.9875
Langmuir	0.48	36.92	0.9020
E-H	0.41	27.39	0.8079

els are given in Table 3.

A low k_m value increases the catalytic efficiency by making the substrate bind more firmly to the enzyme. On the other hand, if k_m is high, the enzyme complex converts the lesser of the substrate into the product [35]. The kinetic parameters in Table 3 indicate that the models (nonlinear and linear) fitted well to the experimental data. However, the linear transformation of the experimental data by the kinetic models of LB, Langmuir, and EF introduces deficiencies that make the linear models prone to error [42]. Untransformed data point estimation through nonlinear regression, allowing direct determination of Eqs. (4) and (5), gives more accurate values for the kinetic parameters [42,43]. Therefore, a reliable estimate of the kinetic parameters (V_{max}=0.15 mmole·L^{-1}min^{-1}, k_m= 43.81 g·L^{-1}) by the m-MM model can be considered the best values under the prevailing experimental conditions.

Carrillo et al. [12] with cellulase enzymes from Novozymes A/S using the modified MM model obtained k_m of 38.2 g·L^{-1} and V_{max} of 0.55 g·L^{-1}h^{-1} for the alkaline pretreatment of wheat straw (6 h for 80 °C) at enzyme hydrolysis conditions of 8 h and 50 °C. The different operating conditions and type of biomass material used in the two studies may have caused a slight difference in values.

2-2. Deactivation and Reactivation Constants

The adsorbed enzymes decrease the concentrations of available adsorption sites with enzymatic reaction progression [44], or it may be said that the deactivation rate is proportional to the concentration of adsorbed enzyme (or the concentration of enzyme in solution but not the product concentration) [10,17]. A rate retarding factor is said to be responsible for the reversible inactivation of the adsorbed enzyme by diffusing into the cellulose fibrils [45]. The first-order decay exponential function of time was used to determine the inactivation and reactivation constants [10]. Applying nonlinear regression analysis, Eq. (17) was used to fit the experimental data to estimate $V_{max,app}$ and k_m values at a specific time for the varying initial substrate concentrations, as shown in Fig. 3. The regressed values for $V_{max,app}$ and k_m are provided in Table 4.

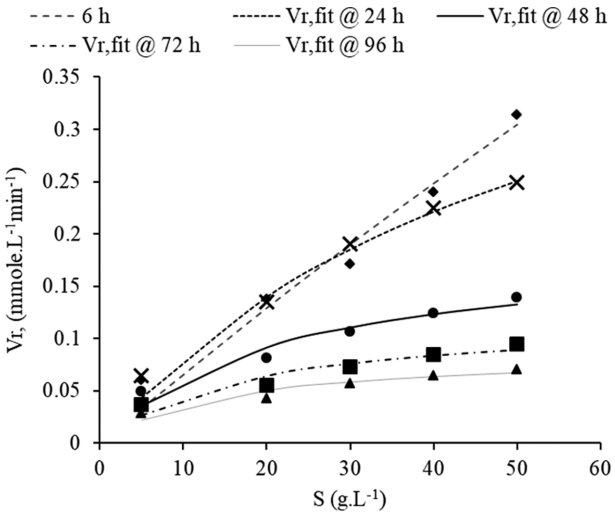

Fig. 3. Real hydrolysis rate from Eq. (17) with varying substrate loadings as a function of reaction time. Markers represent the experimental data.

Table 4. Apparent maximum hydrolysis rate and half-saturation rate constant from Eq. (17)

Time (min)	$V_{max,app}$ (mmole·L^{-1}min^{-1})	k_m (g·L^{-1})	R^2
360	3.20	474.74	0.9756
1,440	0.53	56.48	0.9922
2,880	0.19	21.46	0.9440
4,320	0.12	17.56	0.9106
5,760	0.08	14.76	0.9191

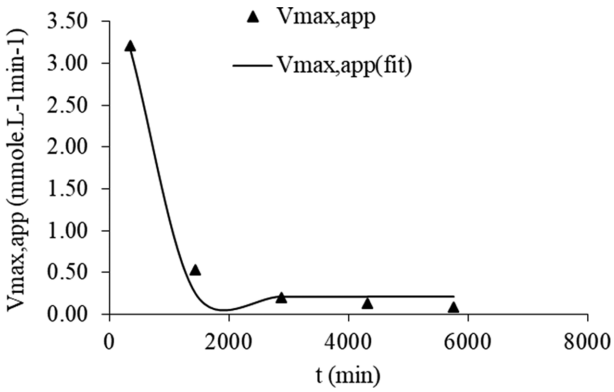

Fig. 4. Apparent maximum hydrolysis reaction rate as a function of time.

The $V_{max,app}$ values as determined from Eq. (17) were used in Eq. (16) to evaluate the inactivation extent (B_0), the residual activity of the enzyme (Z_0), the half-life ($t_{1/2}$), and V_{max}. The inactivation rate constant, k_3, and reactivation rate constant, k_4 were determined from Eqs. (13) to (15). The progression of $V_{max,app}$ with time (Fig. 4) showed a reduction of about 96% during 72 h reaction time and 98% reduction for 96 h reduction time. The results follow similar curves showing a considerable decrease in catalytic constants [10,23].

Fitting Fig. 4 to Eq. (16), the kinetic parameters V_{max}=1.80 mmole·L^{-1}min^{-1}, Z_0=0.12, B_0=6.80, and $t_{1/2}$=174.78 min. The apparent hydrolysis rate, k_2, was calculated by using Eq. (6). The concentration of enzyme added (0.34 mL enzyme to a total reaction volume of 10 mL) was estimated to be 4,166.67 mg·L^{-1}. The average molecular weight of the cellulase enzyme was assumed to be 68,000 g·mole^{-1} (the subunit of the enzyme as provided by Sigma Aldrich is 68 kilo Daltons). Therefore, the total enzyme concentration, $[E]_{total}$ of enzyme used was estimated to be 0.061 mmole·L^{-1}. Using the V_{max} value estimated (1.80 mmole·L^{-1}min^{-1}), k_2 (apparent hydrolysis rate constant) value was 29.51 min^{-1}. Applying the values of Z_0, B_0, and $t_{1/2}$ obtained from Eq.(16) to Eqs. (13), (14), and (15), the inactivation rate constant, k_3=0.269 min^{-1} and the reactivation rate constant, k_4=0.0048 min^{-1}. Since the order of the inactivation rate constant (k_3) is larger than the reactivation rate constant (k_4), an increasing amount of cellulase enzymes becomes inactivated as the enzymatic conversion proceeds [10]. The larger order of k_3 indicates that optimum product formation could be attained at a relatively short enzymatic hydrolysis period and reduced enzyme concentrations. The kinetic parameters obtained in this study are comparable to values reported elsewhere [10,17].

Table 5. Kinetic parameters, k and n, as functions of varying initial enzyme concentrations from Eq. (18)

Enzyme conc., Eo, $g \cdot L^{-1}$	7	14	21	28	35
k ($g \cdot L^{-1}h^{-1}$)	3.26×10^{-4}	2.27×10^{-5}	6.01×10^{-4}	2.04×10^{-5}	7.37×10^{-6}
n	0.65	0.63	0.55	0.49	0.37
R^2	0.9485	0.9488	0.9336	0.9960	0.8428

2-3. Determination of the Diffusion Limit Characteristics

Kinetic parameters that involve diffusion limitation are essential to provide reliable estimates for process behavior [12]. When enzymatic reactions have a diffusion limit, the rate-limiting step can be that substrate diffuses into the active sites, or product diffuses out [35]. This is referred to as kinetic perfection or catalytic perfection [35]. In this wise, the Chrastil model (Eq. (18) was applied to evaluate the diffusion characteristics of the enzymatic process by estimating the parameters k and n [12,17], considering constant initial substrate concentration of 30 $g \cdot L^{-1}$ and varying initial enzyme concentrations (7 to 35 $g \cdot L^{-1}$). The constants were evaluated through nonlinear regression analysis. The values are presented in Table 5.

The n values decreased with increasing enzyme concentration (0.65 to 0.37), which means that the diffusion resistance increased with increasing enzyme concentrations. This increase in diffusion resistance may be due to the molecular steric factor from the enzymes' molecules [12]. As more enzymes get adsorbed to the substrate, a blockage may occur, thereby restricting the diffusion process of the enzymes to the substrate structure [12]. Using this trend, for n values closer to 1, a low-resistance film controls and the reaction is said to be first order. For strongly limited diffusion resistance, n is small (high resistance structure). When n is greater than 1, we may expect a consecutive reaction order [12]. A lower k indicates that the substrate is more resistant to enzymatic hydrolysis, reducing the attack by the enzymes. On the other hand, a higher k value shows the susceptible enzymatic conversion. In this study, the kinetic constant, k, generally decreased in importance with increasing enzyme concentration. This is because, at much higher enzyme concentration, product formation is altered at a maximum, which may be due to enzyme saturation, making the catalytic activity of the enzyme system get reduced. From Table 5, the enzyme concentration of 7 $g \cdot L^{-1}$ has the highest value of 3.26×10^{-4} $g \cdot L^{-1}h^{-1}$ followed by 21 $g \cdot L^{-1}$ enzyme loading (6.01×10^{-4} $g \cdot L^{-1}h^{-1}$). The highest concentration of 35 $g \cdot L^{-1}$ had the lowest value of k (7.37×10^{-6} $g \cdot L^{-1}h^{-1}$).

2-4. Physico-chemical Changes after Raw Biomass Treatments

Stereomicroscopy imaging was used to show size variability and color change after the treatment of the raw corn cob biomass samples. Images showed that biomass particles were reduced in size and more clumped together after the two-stage treatment (Fig. 5(a)-(c)). The enzyme-treated samples (Fig. 5(b)) showed thin and dark small particles (Fig. 5(c)) with more reduced size than the raw and pretreated samples. The APO pretreated samples showed that the initial red color of the raw biomass (Fig. 5(a)) had been bleached by the presence of H_2O_2 in the pretreatment slurry. Scanning electron microscope (SEM) images displayed cell wall distor-

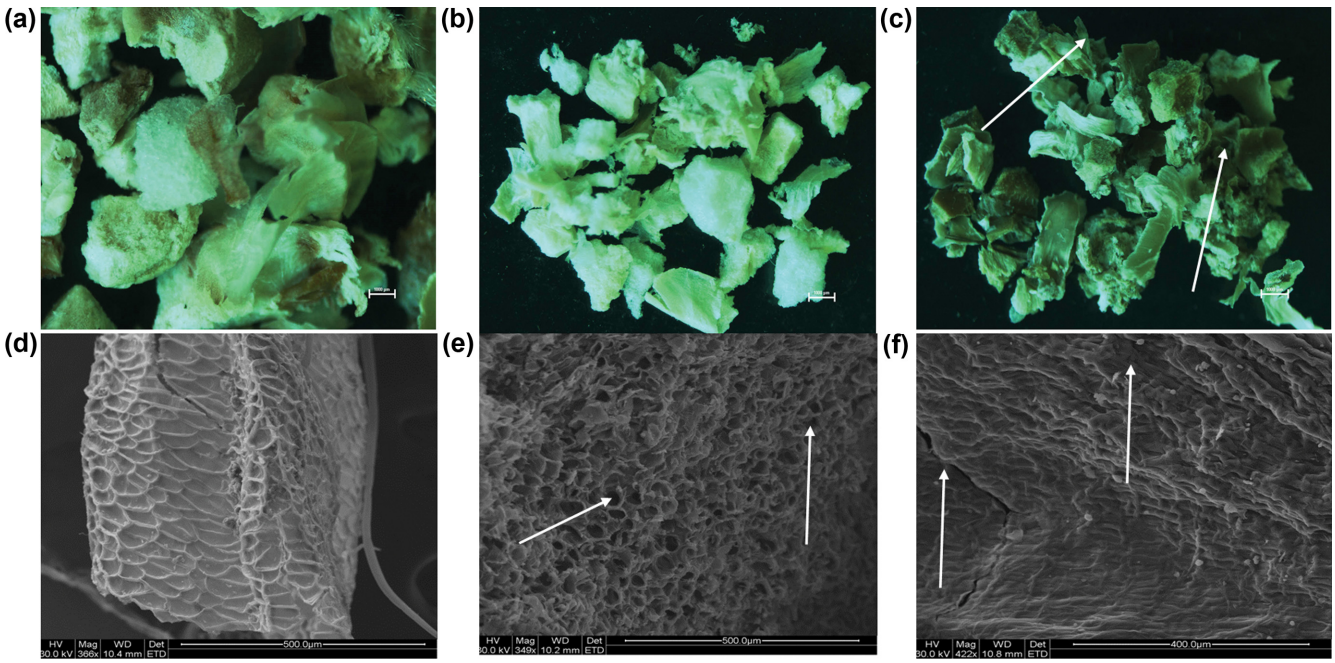

Fig. 5. Micrography images of untreated and treated corn cob. Stereomicrography: (a) Raw biomass, (d) APO pretreatment (c) Enzyme hydrolyzed samples. SEM: (d) Raw biomass, (e) APO pretreated, (f) Enzyme hydrolyzed samples. Arrows show pore openings and reduction in sizes caused by pretreatment and enzymatic hydrolysis of the raw biomass.

Table 6. Infrared crystallinity ratio and hydrogen bond intensity of raw and pretreated biomass

Biomass	Infrared crystallinity ratio		
	α_{1437} cm^{-1}/ α_{899} cm^{-1} (LOI)	α_{1378} cm^{-1}/ α_{2900} cm^{-1} (TCI)	α_{3400} cm^{-1}/ α_{1320} cm^{-1} (HBI)
Raw	0.84	1.06	1.17
Pretreated	0.93	1.02	0.86
Enzyme hydrolyzed	0.90	1.01	0.89

tion and opening of pores (as indicated with arrows) (Fig. 5(d)-(f)). The deformation of the cell walls showed that through the pretreatment and enzyme hydrolysis steps, the microfiber regular arrangements were ruptured and opened up for enzymatic attack (Fig. 5(e)). FTIR spectra [see supplementary file] showed the presence of the functional groups in biomasses. The spectra also revealed that the band intensities were reduced after the APO pretreatment and enzymatic hydrolysis, indicating the reduction of lignin polymer. The ratios of TCI (total crystallinity index), LOI (lateral order index), and HBI (hydrogen bond index) (Table 6), were used to determine crystallinity indices to evaluate the effectiveness of treatments on the raw biomass [35,39]. The peak heights (%Transmittance) were used to determine the ratios (Table 6). Highest TCI and LOI values indicate the highest degree of crystallinity and more ordered cellulose. On the other hand, lowest TCI and LOI values suggest that the cellulose is composed of more amorphous structures, and the lignocellulosic complex has been ruptured, exposing the biomass matrix to the enzyme hydrolysis [39].

CONCLUSION

Accurate prediction has been discussed of kinetic parameters using the existing models and the obtained experimental data for the activation and deactivation of adsorbed cellulase during the enzymatic conversion of alkaline peroxide oxidation pretreated corn cob to sugar. Product formation reached the peak (about 89% conversion yield) at 48 h and 50 $g{\cdot}L^{-1}$ substrate loading. Existing kinetic models such as the classical Michaelis-Menten, Lineweaver-Burke, Langmuir, Eadie-Hofstee, and modified Michaelis-Menten were investigated. Decline in the enzyme activity could be explained by considering the apparent hydrolysis rate, inactivation, and reactivation of the adsorbed enzyme using relevant kinetic models. Reliable estimate of the kinetic parameters (V_{max}=0.15 $mmole{\cdot}L^{-1}min^{-1}$, k_m=43.81 $g{\cdot}L^{-1}$) was correlated by the modified Michaelis-Menten model. Regressed values of apparent maximum rate, $V_{max,app}$, for adsorbed enzymes reduced appreciably with time from 3.20 $mmole{\cdot}L^{-1}min^{-1}$ to 0.08 $mmole{\cdot}L^{-1}min^{-1}$ (about 98%) at 96 h. Furthermore, findings of this study indicate that as the enzymatic reaction progressed with increasing enzymes concentration, the activity of the enzyme decreased.

NOMENCLATURE

A_o : inactivation extent
E_o : initial enzyme concentration $[g{\cdot}L^{-1}]$
$[E]_{total}$: total enzyme concentration $[mmole{\cdot}L^{-1}]$
V_o : initial hydrolysis rate $[mmole{\cdot}L^{-1}min^{-1}]$
y_o : residual enzyme activity
V_{max} : maximum initial hydrolysis rate $[mmole{\cdot}L^{-1}min^{-1}]$
$V_{max,app}$: apparent maximum initial hydrolysis rate $[mmole{\cdot}L^{-1}min^{-1}]$
V_r : real hydrolysis rate $[mmole{\cdot}L^{-1}min^{-1}]$
$t_{1/2}$: half-life [min]
P : product concentration $[g{\cdot}L^{-1}]$
P_σ : products that diffused at equilibrium $[g{\cdot}L^{-1}]$
S : substrate concentration $[g{\cdot}L^{-1}]$
k : diffusion coefficient for adsorption $[g{\cdot}L^{-1}{\cdot}h^{-1}]$
k_m : half-maximum initial hydrolysis rate $[g{\cdot}L^{-1}]$
k_2 : apparent hydrolysis rate constant $[min^{-1}]$
k_3 : inactivation rate constant $[min^{-1}]$
k_4 : reactivation rate constant $[min^{-1}]$
n : structural diffusion resistance constant

SUPPORTING INFORMATION

Additional information as noted in the text. This information is available via the Internet at http://www.springer.com/chemistry/journal/11814.

REFERENCES

1. G. Y. Yew, S. Y. Lee, P. L. Show, Y. Tao, C. L. Law, T. T. C. Nguyen and J. S. Chang, *Bioresour. Technol. Rep.*, **7**, 100227 (2019).
2. Y. Liu, W. Han, X. Xu, L. Chen, J. Tang and P. Hou, *Biochem. Eng. J.*, **156**, 107528 (2020).
3. S. Takkellapati, T. Li and M. A. Gonzalez, *Clean Technol. Environ. Policy*, **20**, 1615 (2018).
4. P. K. Dikshit, H.-B. Jun and B. S. Kim, *J. Chem. Eng.*, **37**, 387 (2020).
5. S. Liu and Q. Wang, *Cellulose Chem. Technol.*, **50**, 803 (2016).
6. A. T. Adeleye, H. Louis, O. U. Akakuru, I. Joseph, O. C. Enudi and D. P., *AIMS Energy*, **7**, 165 (2019).
7. M. M. H. Coelho, N. W. S. Morais, E. L. Pereira, R. C. Leitão and A. B. dos Santos, *Biochem. Eng. J.*, **156**, 107502 (2020).
8. A. I. Adeogun, B. E. Agboola, M. A. Idowu and T. A. Shittu, *J. Bioresour. Bioprod.*, **4**, 149 (2019).
9. A. O. Ayeni and M. O. Daramola, *J. Environ. Chem. Eng.*, **5**, 1771 (2017).
10. Y. Zhuoliang and R. E. Berson, *Bioresour. Technol.*, **102**, 11194 (2011).
11. E. I. Makarova, V. V. Budaeva, A. A. Kukhlenko and S. E. Orlov, *3 Biotech*, **7**, 317 (2017).
12. F. Carrillo, M. J. Lis, X. Colom, M. López-Mesas and J. Valldeperas, *Process Biochem.*, **40**, 3360 (2005).
13. W. Lin, S. Xing, Y. Jin, X. Lu, C. Huang and Q. Yong, *Bioresour. Technol.*, **306**, 123163 (2020).
14. N. M. Jamil, *WIT Trans. Ecol. Environ.*, **186**, 499 (2014).
15. M. L. Carvalho, R. Sousa Jr., U. F. Rodríguez-Zúñiga, C. A. G. Suarez, D. S. Rodrigues, R. C. Giordano and R. L. C. Giordano, *Braz. J. Chem. Eng.*, **30**, 437 (2013).
16. R. S. Ghadge, A. W. Patwardhan, S. B. Sawant and J. B. Joshi, *Chem. Eng. Sci.*, **60**, 1067 (2005).

17. A. O. Converse, R. Matsuno, M. Tanaka and M. Taniguchi, *Biotechnol. Bioeng.*, **32**, 38 (1988).
18. Y. Zhang, J.-L. Xu, H.-J. Xu, Z.-H. Yuan and Y. Guo, *Bioresour. Technol.*, **101**, 8261 (2010).
19. C. Huang, W. Lin, C. Lai, X. Li, Y. Jin and Q. Yong, *Bioresour. Technol.*, **285**, 121355 (2019).
20. J. Jalak and P. Valjamae, *Biotechnol. Bioeng.*, **106**, 871 (2010).
21. S. Peri, S. Karra, Y. Y. Lee and M. N. Karim, *Biotechnol. Prog.*, **23**, 626 (2007).
22. Q. Gan, S. J. Allen and G. Taylor, *Process Biochem.*, **38**, 1003 (2003).
23. J. A. Asenjo, *Biotechnol. Bioeng.*, **25**, 3185 (1983).
24. J. Hong, X. H. Ye and Y. H. P. Zhang, *Langmuir*, **23**, 12535 (2007).
25. G. E. Briggs and J. B. Haldane, *Biochem. J.*, **19**, 338 (1925).
26. J. Chrastil and J. T. Wilson, *Int. J. Biochem.*, **14**, 1 (1982).
27. J. Chrastil, *Int. J. Biochem.*, **20**, 683 (1988).
28. J. M. Gould, *Biotechnol. Bioeng.*, **26**, 46 (1984).
29. A. O. Ayeni, J. A. Omoleye, S. Mudliar, F. K. Hymore and R. A. Pandey, *Korean J. Chem. Eng.*, **31**, 1180 (2014).
30. G. L. Miller, *Anal. Chem.*, **31**, 426 (1959).
31. A. O. Ayeni, J. A. Omoleye, F. K. Hymore and R. A. Pandey, *Braz. J. Chem. Eng.*, **33**, 33 (2016).
32. C. G. Yoo, C. W. Lee and T. H. Kim, *Biomass Bioenergy*, **35**, 4901 (2011).
33. M. A. Lemos, J. A. Teixeira, M. R. M. Domingues, M. Mota and F. M. Gama, *Microb. Technol.*, **32**, 35 (2003).
34. D. Lloyd, *J. Mol. Evolut.*, **45**, 370 (1997).
35. J. Bian, F. Peng, X.-P. Peng, P. Peng, F. Xu and R.-C. Sun, *Bioresour.*, **7**, 4626 (2012).
36. J. M. Berg, *Biochemistry*, W.H. Freeman, New York (2007).
37. J. Crank, *The mathematics of diffusion*, Clarendon Press, Oxford (1975).
38. A. O. Ayeni, M. O. Daramola, A. Awoyomi, F. B. Elehinafe, A. Ogunbiyi, P. T. Sekoai and J. A. Folayan, *Cogent Eng.*, **5**, 1509665 (2018).
39. I. Spiridon, C. Teacă and R. Bodîrlău R, *Bioresour.*, **6**, 400 (2011).
40. J. S. Gratzl, *Papier*, **46**, 1 (1992).
41. P. Valjamae, V. Sild, G. Pettersson and G. Johansson, *Eur. J. Biochem.*, **253**, 469 (1998).
42. M. Marasovi, T. Marasovi and M. Miloš, *J. Chem.*, **6560983**, 1 (2017).
43. G. N. Wilkinson, *Biochem. J.*, **80**, 324 (1961).
44. M. T. Holtzapple, H. S. Caram and A. E. Humphrey, *Biotechnol. Bioeng.*, **26**, 775 (1984).
45. R. Matsuno, M. Taniguchi, M. Tanaka and T. Kamikubo, *Enz. Eng.*, **7**, 158 (1984).